ACS APPLIED MATERIALS & INTERFACES

Research Article

www.acsami.org

Yolk–Shell $Fe^0@SiO_2$ Nanoparticles as Nanoreactors for Fenton-like Catalytic Reaction

Chao Liu, Jiansheng Li,* Junwen Qi, Jing Wang, Rui Luo, Jinyou Shen, Xiuyun Sun, Weiqing Han, and Lianjun Wang*

Jiangsu Key Laboratory of Chemical Pollution Control and Resources Reuse School of Environmental and Biological Engineering, Nanjing University of Science and Technology, Nanjing 210094, People's Republic of China

Supporting Information

ABSTRACT: Yolk–shell nanoparticles (YSNs) with active metal cores have shown promising applications in nanoreactors with excellent catalytic performance. In this work, $Fe^0@SiO_2$ YSNs were synthesized by a sequential "two-solvents" impregnation–reduction approach. Specifically, $FeSO_4$ aqueous solution was introduced into the preformed hollow mesoporous silica spheres (HMSS), dispersed in *n*-hexane, via a "two-solvent" impregnation way. Subsequently, aqueous solution of sodium borohydride ($NaBH_4$) was introduced into the cavity of HMSS by the same way, leading to the formation of Fe core inside the HMSS through the reaction between Fe^{2+} and $NaBH_4$. The resulting $Fe^0@SiO_2$ YSNs possess distinctive structures, including active cores, accessible mesoporous channels, protective shells, and hollow cavities. To present the catalytic performance of YSNs nanoreactors, Fenton-like catalytic oxidation of phenol was chosen as the model catalysis reaction. In addition to the $Fe^0@SiO_2$ YSNs, two other materials were also applied to the catalytic system for comparison, including $Fe@SiO_2$ composites with iron nanoparticles sticking on the outer shells of HMSS ($Fe@SiO_2$-DI) and bare iron nanoparticles without HMSS (bare Fe^0), respectively. The catalytic results show that $Fe^0@SiO_2$ YSNs exhibit higher catalytic rate toward phenol removal at 2-fold and 4-fold as compared to that of $Fe@SiO_2$-DI and bare Fe^0, indicating the outstanding catalytic property of YSNs nanoreactors. To further clarify the relationship between catalytic properties and structural characteristics, the adsorption experiments of the three samples were also performed in the absence of H_2O_2. Other than catalytic results, $Fe^0@SiO_2$ YSNs show slightly higher adsorption efficiency than the other two samples, indicating the accessibility of nanoreactors. This result demonstrates that the removal of phenol in the oxidation system of $Fe^0@SiO_2$ YSNs may have contributed to the structure-enhanced effect of YSNs as nanoreactors.

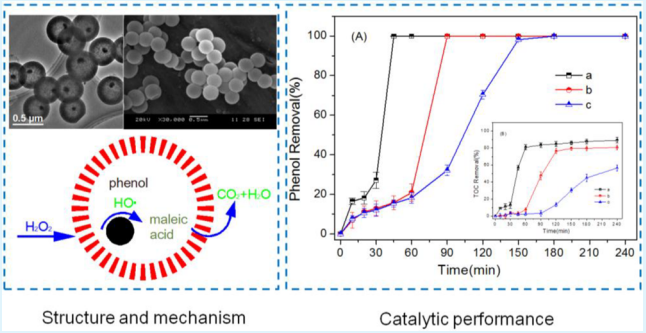

KEYWORDS: *yolk–shell, nanoreactor, "two-solvents" impregnation–reduction, Fenton-like catalysis, structure-enhanced effect*

1. INTRODUCTION

In the past few decades, yolk–shell nanoparticles (YSNs), which show a characteristic core@void@shell architecture, have received considerable attention.[1−3] With the appealing structures of movable cores, interstitial hollow spaces between the movable core and shell sections, and the functional shells, YSNs have played important roles in modern science and technology as promising candidates for emerging applications, such as nanoreactors,[4−12] lithium-ion batteries,[13−15] drug delivery,[16,17] surface-enhanced Raman scattering,[18,19] and sensors.[20]

Motivated by their promising prospects, great efforts have been devoted to the preparation of YSNs.[7,21−28] In most synthetic methods, performed core has been used as the seed for YSNs. After coating or double-coating different materials on the cores using hard or soft templating approaches, the YSNs were produced by selectively etching the cores or removing the middle layers.[17,21,29−31] The so-called "pre-core to post-shell" methods are in general complicated and often need strong acids in formation of YSNs. Recently, a new "pre-shell to post-core" route has been reported by some groups,[7,32−34] in which the core was introduced into the preformed shell of hollow spheres. For example, $Cu@SiO_2$ YSNs[32] and $Fe_2O_3@SiO_2$ YSNs[7] were synthesized by introducing corresponding metal salt into the cavity of the hollow silica spheres. In these processes, vacuum, sonication, long-time mixing, and the removal of unreacted metal salts were needed for the incorporation of active species into hollow spheres. Hence, it is highly desirable to employ a simple, controllable, and efficient way for the introduction of active cores into hollow spheres.

Since the pioneering work by Anne et al. on the synthesis of MnO_2 loaded SBA-15,[35] a "two-solvents" method has been developed as a frequently used impregnation technique to load guest species into two-dimension mesoporous silica (TDMS)

Received: May 18, 2014
Accepted: July 21, 2014
Published: July 22, 2014

materials. This method promotes the loading of the pores of TDMS with a metal salt solution, by prewetting the silica materials with a hydrophobic alkane solvent (i.e., *n*-hexane, *n*-pentane, or cyclohexane).[36] Up to now, a variety of TDMS-based nanocomposites, with metal oxide inside the mesoporous silica grains, have been fabricated by this approach.[36−43] Generally, no operations such as vacuum, sonication, or long-time mixing were involved in the "two-solvents" method. Meanwhile, the whole process was controllable and efficient.[36,39] However, this method has not been used for the construction of YSNs with active cores.

Herein, we successfully prepared a $Fe^0@SiO_2$ yolk−shell nanostructure by a sequential "two-solvents" impregnation−reduction approach. In the synthetic process, $FeSO_4$ aqueous solution was introduced into the preformed hollow mesoporous silica spheres (HMSS), dispersed in *n*-hexane, via a "two-solvent" impregnation way. Subsequently, aqueous solution of sodium borohydride ($NaBH_4$) was introduced into the cavity of HMSS by the same way. The Fe core was formed inside the HMSS through the reaction between Fe^{2+} and $NaBH_4$. To present the catalytic performance of YSNs nanoreactors, Fenton-like catalytic oxidation of phenol was chosen as the model catalysis reaction. Except for the $Fe^0@SiO_2$ YSNs, two other materials were also applied to the catalytic reaction for comparison, including $Fe@SiO_2$ composites with iron nanoparticles sticking on the outer shells of HMSS and bare iron nanoparticles, respectively. To further demonstrate the structure-enhanced effect of YSNs as nanoreactors, the adsorption properties of the three samples were also investigated in the absence of H_2O_2.

2. EXPERIMENTAL SECTION

2.1. Chemicals and Materials. Anhydrous ethanol, concentrated ammonia aqueous solution (25 wt %), tetraethoxysilane (TEOS), sodium borohydride, methanol, *n*-hexane, and ferrous sulfate heptahydrate were purchased from Sinopharm Chemical Reagent Co., Ltd. Cetyltrimethylammonium bromide (CTAB) was purchased from Chengdu Kelong Chemical Co., Ltd. All chemicals were used as received without any further purification. Millipore water was used in all experiments.

2.2. Synthesis of Hollow Mesoporous Silica Spheres. Hollow mesoporous silica spheres (HMSS) were synthesized by a reported method.[44] The typical preparation of HMSS was described by the following procedure. 0.168 g of CTAB was added to a solution containing deionized water, anhydrous ethanol, and ammonia solution (25 wt %). The resulting mixture was heated to 35 °C, and 1 mL of TEOS was added under vigorous stirring. The molar ratio of the reaction mixture was $1.00TEOS:0.092C_{16}TAB:2.96NH_3:621H_2O:79C_2H_5OH$. After being stirred at 35 °C for 24 h, the white product was collected by centrifugation at 5000 rpm for 10 min and washed three times with ethanol. The as-made Stöber silica spheres then were incubated in 160 mL of pure water at 70 °C for 12 h and collected by centrifugation after washing three times with ethanol. Subsequently, the as-synthesized HMSS were dried and calcined at 550 °C in air, donated as blank HMSS.

2.3. Synthesis of $Fe^0@SiO_2$ YSNs. The $Fe^0@SiO_2$ YSNs were prepared through a sequential "two-solvents" impregnation−reduction approach. In a typical experiment, 1 g of HMSS was added into 30 mL of *n*-hexane with stirring until the HMSS were well dispersed. Next, 60 μL of $FeSO_4$ aqueous solution (2.4 M) was added dropwise with stirring for 1 h. The mass ratio of Fe/SiO_2 was 0.08. Next, $NaBH_4$ aqueous solution was added under N_2 atmosphere. The molar ratio of B/Fe was 4/1 with adequate $NaBH_4$ for the growth of iron nanoparticles. The obtained $Fe^0@SiO_2$ YSNs were collected by a magnet and washed with methanol for three times. The final products were denoted as $Fe^0@SiO_2$ YSNs.

2.4. Synthesis of $Fe^0@SiO_2$ Composites. The $Fe^0@SiO_2$ composites were prepared by a direct impregnation method. Briefly, 1 g of HMSS was added into 5 mL of $FeSO_4$ aqueous solution with stirring for 12 h. The mass ratio of Fe/SiO_2 was 0.08. The suspension then was dried under vacuum at 45 °C, followed by the addition of 10 mL of $NaBH_4$ aqueous solution with stirring. The molar ratio of B/Fe was 4/1. The following procedure was the same as above. The resulted products were denoted as $Fe^0@SiO_2$-DI.

2.5. Synthesis of Fe^0 Nanoparticles. The Fe^0 nanoparticles were prepared with a simple liquid-phase reduction method. In a typical procedure, 0.4 M $NaBH_4$ aqueous solution was added dropwise to a 0.1 M $FeSO_4$ aqueous solution under N_2 atmosphere. The molar ratio of B/Fe was 4/1. The rest of the procedure was repeated as above. The black products were denoted as bare Fe^0.

2.6. Characterization. The X-ray diffraction (XRD) patterns were recorded on a Bruker AXS D 8 advance powder diffraction system using Cu Kα (λ = 1.5418 Å) radiation. The XPS spectra were obtained by using a PHI Quantera II ESCA System with Al Kα radiation at 1486.8 V. Scanning electron microscopy (SEM) images were collected on a JEOL JSM-6380LV microscope using gold-coated powder specimens. Transmission electron microscopy (TEM) images were obtained using a JEOL JEM-2100 microscope, operating at 200 kV. N_2 adsorption/desorption isotherms were measured using Micromeritics ASAP-2020 at liquid nitrogen temperature (−196 °C).

2.7. Catalytic Experiments. In a typical procedure, a given amount of catalyst with equivalent Fe^0 (2 mg of bare Fe^0, 27 mg of Fe^0/SiO_2-DI containing 2 mg of Fe^0, or 27 mg of Fe^0/SiO_2 YSNs containing 2 mg of Fe^0) was slurried to a sealed conical flask containing 25 mL of phenol solution (100 ppm). All conical flasks were kept in a horizontal vibrator and shaken at 200 rpm at 60 °C. Subsequently, the required amounts of hydrogen peroxide (0.304 mL, 30%) were added to initiate the catalytic reaction. At the given time, aliquots were withdrawn and filtered through a 0.45 μm syringe-driven filter. The phenol concentrations of the samples were determined by high-performance-liquid chromatography (HPLC, Water 1525). The total organic carbon (TOC) contents of the samples were measured by TOC analyzer (Vario TOC Cube, Elementar Analysensyteme GrmbH). The adsorption experiments were performed in the absence of H_2O_2, while the other conditions were not changed as compared to the catalytic experiments.

3. RESULTS AND DISCUSSION

Figure 1 shows the low-angle and wide-angle XRD patterns of all samples. Except for the bare Fe^0 with no obvious peak (Figure 1A), the other products exhibit an intense reflection at low 2θ, which are typical of worm-like pore structures and are similar to the previous works.[45,46] Obviously, the introduction of Fe has no apparent effect on the mesoporous structure of HMSS.

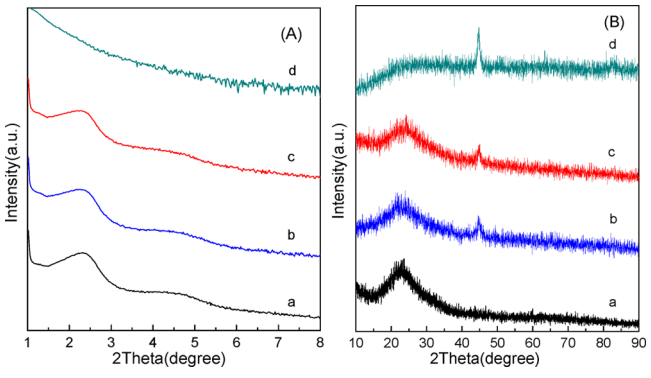

Figure 1. (A) Small-angle and (B) wide-angle XRD patterns of (a) blank HMSS, (b) $Fe^0@SiO_2$ YSNs, (c) $Fe^0@SiO_2$-DI, and (d) bare Fe^0.

The formation of Fe^0 particles was confirmed by wide-angle XRD (Figure 1B). In the pattern of blank HMSS, only one broad peak corresponding to amorphous silica at 22.8° can be observed. For three iron-containing samples, an obvious diffraction peak at 44.6° can be observed, which is in accordance with the 110 diffraction of body-centered cubic α-Fe (JCPDS no. 06-0696). As compared to bare Fe^0, it can be seen that the diffraction peak becomes weaker and broader with the addition of HMSS in two $Fe@SiO_2$ samples, indicating that the crystal size of the iron particles in the two $Fe@SiO_2$ samples is reduced.

As we know, Fe^0 can be oxidized easily when exposed in air. Thus, XPS was used to investigate the composition of iron in three iron-containing samples (Figure 2). The photoelectron

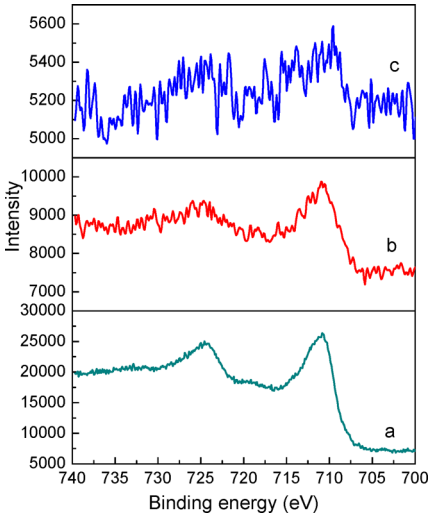

Figure 2. XPS spectra of Fe 2p region: (a) bare Fe^0, (b) $Fe^0@SiO_2$-DI, and (c) $Fe^0@SiO_2$ YSNs.

peaks at 711 and 724.6 eV represent the binding energies of Fe $2p_{3/2}$ and $2p_{1/2}$, respectively, indicating the existence of a layer of iron oxides.[47] However, no Fe^0 was detected in the samples. This result differs from that measured by XRD, probably due to the fact that XPS probes the near surface region within about 3−5 nm.[48] The limited probe depth of XPS eliminates any information from the bulk solid phase, resulting in no characteristic doublet of Fe^0. Moreover, the intensity of Fe 2p in $Fe^0@SiO_2$ YSNs was much weaker than that of $Fe^0@SiO_2$-DI, which can contribute to the isolation of silica shells, further indicating that iron nanoparticles in $Fe^0@SiO_2$ YSNs sample were mainly inside the cavity of HMSS.

To find direct proof of the existence of Fe^0 in the sample, the HRTEM observation was conducted, and the images are shown in Supporting Information Figure S1. From Supporting Information Figure S1(a), it can be seen that the particle is covered by an iron oxide shell with the thickness of 6.1 nm. Considering the limited probe depth of XPS for Fe 2p photoelectrons is ∼3−5 nm,[48] the present of the oxide shell is responsible for the lack of Fe^0 peak in the XPS spectra. The HRTEM image (Supporting Information Figure S1(b)) illustrates the perfect arrangement of the atomic layers and lack of defects. The lattice plane distance in the image is 2.03 Å, which is consistent with the [110] plane of the α-Fe (JCPDS card no. 06-0696). The results are well in agreement with those of the XRD and XPS analyses.

SEM was employed to study the size and morphology of the products (Figure 3). The as-synthesized HMSS have a spherical

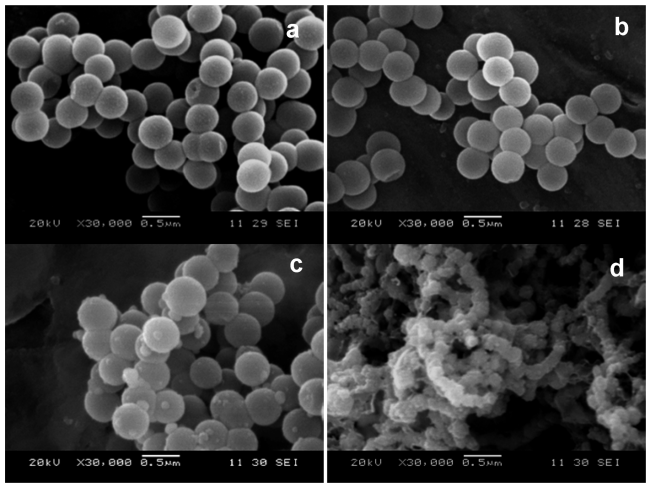

Figure 3. SEM images of (a) blank HMSS, (b) $Fe^0@SiO_2$ YSNs, (c) $Fe^0@SiO_2$-DI, and (d) bare Fe^0.

morphology with smooth surface and uniform diameter of about 400 nm (Figure 3a). After incorporation of Fe^0 cores by the sequential "two-solvents" impregnation−reduction approach, the $Fe^0@SiO_2$ YSNs retain the morphology and size of HMSS, with barely Fe particles on the outer shells (Figure 3b). The image of $Fe@SiO_2$-DI is shown in Figure 3c. Although the spherical morphology is kept, many particles of iron can be observed, sticking on the outer shell of HMSS or even out of the spheres. It is concluded that the sequential "two-solvents" impregnation−reduction approach is important to load Fe^0 nanoparticles inside HMSS. In comparison with the images of $Fe^0@SiO_2$-DI (Figure 3c) and $Fe^0@SiO_2$ YSNs (Figure 3b), it can be seen that the bare iron particles are seriously aggregated in the image of bare Fe^0.

To further investigate the mesostructure and interior construction of the as-synthesized materials, TEM images have been shown in Figure 4. A noticeable contrast between the cavity and the shell is observed in Figure 4a, c, and d, which verify the hollow structure of HMSS. The cavity of HMSS provides the void for the introduction of Fe^0 core and also a confined nanospace for the catalytic reaction. It can also be observed that the HMSS have a mean shell thickness of 80 nm and an average diameter of about 400 nm, which is consistent with the results of SEM. The high-magnification TEM image of HMSS (Figure 4b) reveals that the shells of HMSS display worm-like mesoporous structure, similar to mesoporous molecular sieve silicas with wormhole framework structures.[45] The mesochannels of the HMSS are radially oriented to the sphere surface, which make the molecules easily penetrate the shell and reach the Fe core. As direct evidence for yolk−shell structure, the TEM image of $Fe^0@SiO_2$ YSNs is presented in Figure 4c. The yield of the product is very high, and almost each iron particle, with a size of ∼75 nm, is encapsulated by a shell with a thickness of ∼80 nm. At the same time, barely any Fe particles are formed in the mesochannels. However, for sample $Fe@SiO_2$-DI by the direct impregnation method, it can be seen that some Fe^0 nanoparticles adhere to the outer surface of the shells (Figure 4d). Similar to $Fe^0@SiO_2$ YSNs, the Fe^0 particles barely exist in the mesochannels of HMSS in $Fe@SiO_2$-DI. In Supporting Information Figure S2 of bare Fe^0, a

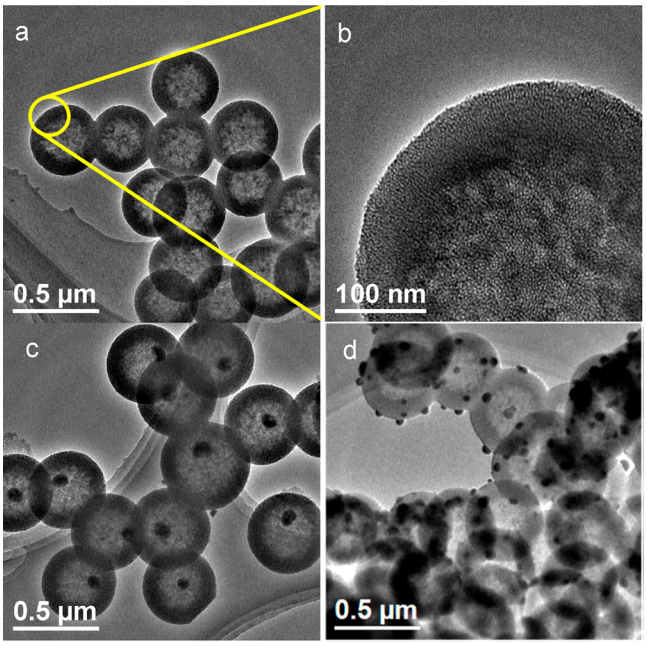

Figure 4. TEM images of (a) blank HMSS, (b) high-magnification TEM image of HMSS, (c) $Fe^0@SiO_2$ YSNs, and (d) $Fe^0@SiO_2$-DI.

serious aggregation of Fe^0 particles happens without the addition of HMSS. The results obtained from TEM were consistent with the SEM characterization. Therefore, $Fe^0@SiO_2$ YSNs via sequential "two-solvents" impregnation−reduction approach are able to provide more exposed active sites for catalysis reaction. Meanwhile, the enhanced dispersibility of iron nanoparticles with the existence of HMSS can also improve the reaction activity.

Figure 5A shows the nitrogen adsorption−desorption isotherms of the as-synthesized materials. Besides the bare Fe^0, the other samples exhibit a type IV isotherm with a type H_2 hysteresis loop, characteristic of mesoporous structure. Such observations further confirm that the incorporation of Fe^0 cannot break the structure of HMSS, consistent with the results of XRD and TEM. Although the introduction of Fe^0 has a negligible effect on the mesoporous feature of HMSS, a perceptible reduction of pore structure parameters can be observed. The BET surface area and pore volume of $Fe^0@SiO_2$ YSNs ($707 m^2 g^{-1}$, $0.46 cm^3 g^{-1}$) and $Fe^0@SiO_2$-DI ($652 m^2 g^{-1}$, $0.42 m^3 g^{-1}$) are lower than those of blank HMSS ($760 m^2 g^{-1}$, $0.51 cm^3 g^{-1}$), which should be contributed to the increment of sample density after loading Fe. The pore size distribution derived from the adsorption branch for all samples is shown in Figure 5B. Except for the bare Fe^0, the other samples show a primary mesoporous size centered at 2.5 nm. It is noteworthy that, after the "two-solvent" reduction and direct impregnation processes, the Fe^0/SiO_2 composites retain the same pore size. Therefore, $Fe^0@SiO_2$ YSNs have been successfully prepared through a sequential "two-solvents" impregnation−reduction approach. We also believe that the sequential "two-solvents" impregnation−reduction approach method may be versatile and could synthesize a wide range of yolk−shell structures with different cores. For example, Au nanoparticles can also be incorporated into the HMSS in the same way (Figure S3, Supporting Information).

The degradation of aromatic pollutants present in wastewater generated by industrial processes has emerged as an important concern over the past years.[49] Heterogeneous Fenton-like catalysts have been promising candidates for the degradation of aromatic pollutants.[6,50] Recently, Fe^0-based materials are commonly used as catalysts for Fenton-like reaction with relatively high activities. In this study, Fenton-like reactions were carried out for phenol degradation to explore the activities of bare Fe^0, $Fe^0@SiO_2$-DI, and $Fe^0@SiO_2$ YSNs. The initial pH value of the reaction solution was 5.6 without the adjustment by additional acid or base. All of the reactions were carried out in the dark to avoid the impact of light. The catalytic oxidation process occurring in the $Fe^0@SiO_2$ YSNs is illustrated in Scheme 1. Reactants, such as phenol and H_2O_2, diffuse through

Scheme 1. Catalytic Oxidation Process

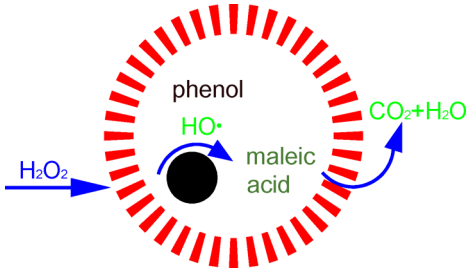

the mesochannels, enter inside the hollow cavity, and then reach the Fe cores. Subsequently, the Fe^0 cores and H_2O_2 produce hydroxyl radical with high reactivity,[51] which accelerate the degradation of phenol to intermediate products and final

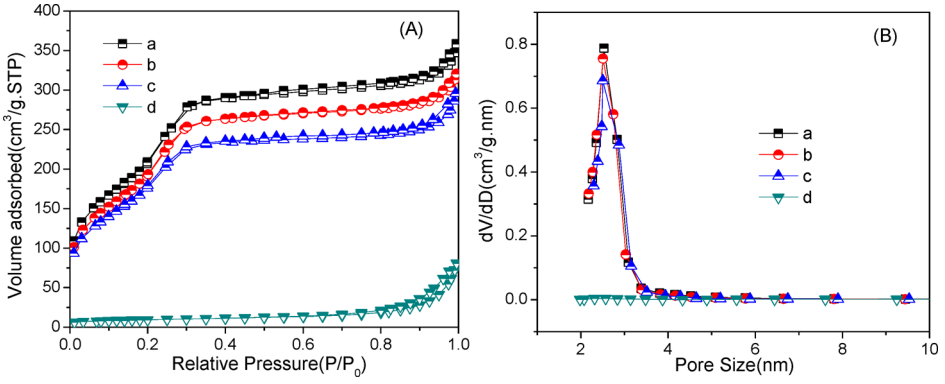

Figure 5. N_2 adsorption/desorption isotherms (A) and pore size distributions (B) of (a) blank HMSS, (b) $Fe^0@SiO_2$ YSNs, (c) $Fe^0@SiO_2$-DI, and (d) bare Fe^0.

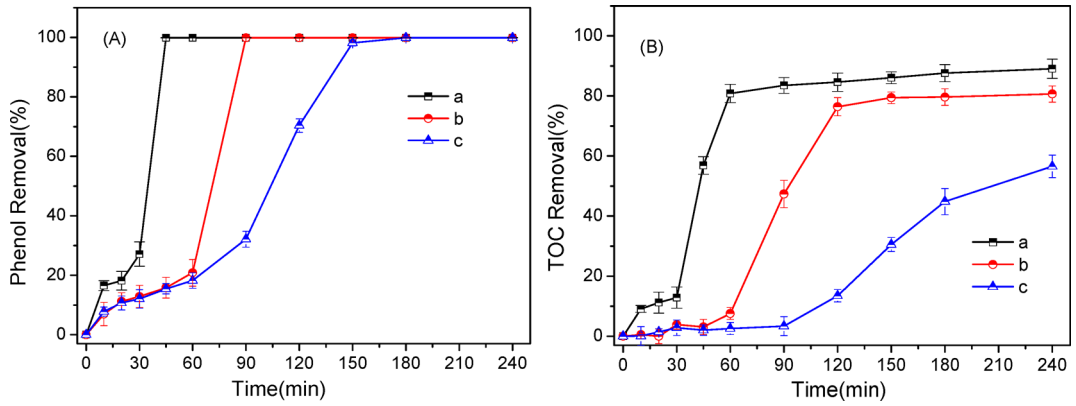

Figure 6. (A) Phenol removal ratio and (B) TOC removal ratio of (a) $Fe^0@SiO_2$, YSNs (b) $Fe^0@SiO_2$-DI, and (c) bare Fe^0.

mineralization. The catalytic reaction is confined inside the hollow space of $Fe^0@SiO_2$ YSNs, which may mainly contribute to the excellent catalytic performance.[52]

The degradation process of phenol catalyzed by $Fe^0@SiO_2$ YSNs was demonstrated by HPLC (Supporting Information Figure S4(A)). As shown in Figure 6A, $Fe^0@SiO_2$ YSNs show the highest activity, and 99.9% of the phenol was oxidized in 45 min, while only 15.8% for $Fe^0@SiO_2$-DI and 15.4% for bare Fe^0. The removal ratio of phenol for $Fe^0@SiO_2$-DI and bare Fe^0 reached 99.9% in 90 and 180 min, respectively. Therefore, $Fe^0@SiO_2$-DI shows higher reactivity than bare Fe for phenol degradation. The poor catalytic reactivity of bare Fe may have contributed to the serious aggregation of iron nanoparticles, based on the SEM and TEM images. Moreover, the enhanced catalytic reactivity of $Fe^0@SiO_2$ YSNs than $Fe^0@SiO_2$-DI may benefit from the nanoreactor feature of the yolk−shell structure. To demonstrate the degree of mineralization of the three catalysts for phenol, the removal ratio of TOC is shown in Figure 6B. Similarly, 81% of phenol was degraded to water and CO_2 within 60 min through the catalysis of $Fe^0@SiO_2$ YSNs, and finally the removal ratio of TOC reached up to 89% in 6 h. For comparison, the TOC values of $Fe^0@SiO_2$-DI and bare Fe^0 were only reduced by 8% and 3% within 60 min, respectively. Eventually, the values reached 80% and 56% in 6 h relative to the original solution. The mineralization rate of $Fe^0@SiO_2$ YSNs was much faster than those of $Fe^0@SiO_2$-DI and bare Fe^0. Clearly, $Fe^0@SiO_2$ YSNs possessed more effective and thorough mineralization for phenol removal than the other two samples, indicating the outstanding catalytic property of YSNs nanoreactors.

To investigate the intermediate products, HPLC was used to analyze the solutions after Fenton-like catalysis. It is confirmed that the mainly intermediate product from phenol is maleic acid (Supporting Information Figure S5). At the same time, an encouraging phenomenon was found: when $Fe^0@SiO_2$-DI and bare Fe^0 were utilized as Fenton catalysts, three different products were detected in the corresponding solutions. However, when $Fe^0@SiO_2$ YSNs were used, only one kind of product existed in the reaction system (Supporting Information Figure S4(B)). It can be concluded that the $Fe^0@SiO_2$ YSNs show an enhanced selective catalysis for phenol degradation to maleic acid, which may have contributed to the confined effect of YSNs nanoreactors. As is known, YSNs with interior void can be used as nanoreactors in which chemical reaction processes may present vast differences because of the confining effect and change in microenvironment.[53]

The outstanding catalytic performance of $Fe^0@SiO_2$ YSNs nanoreactor was attributed to the following reasons. In the catalytic system of $Fe^0@SiO_2$ YSNs nanoreactors, the metal Fe nanoparticles show smaller particle size and enhanced dispersion inside the cavity, which may have contributed to the isolation of HMSS. Therefore, the iron cores may provide more exposed active sites for catalysis reactions. Moreover, phenol molecules were able to facilely diffuse through the mesoporous silica shells and enter inside the hollow space of the nanoreactor. The conversion of phenol molecules leads to a lower reactant concentration and a higher product concentration in the hollow space. The difference of their concentrations inside and outside facilitates phenol molecules continuing to go inside and products coming out from the hollow space, which guarantees the continuity of the catalytic reaction. The catalytic reactions were confined inside the hollow cavity, where the Fe core was more accessible to the reactant. The confinement effect also ensures the target molecules to be reacted as completely as possible.

To further demonstrate the relationship between catalytic properties and structural characteristics, the adsorption experiments of the three materials were also performed in the absence of H_2O_2, while the other conditions were not changed as compared to the catalytic experiments (Figure 7). As can be seen from the adsorption curves, 5.5% and 5.0% of phenol were adsorbed by $Fe^0@SiO_2$ YSNs and $Fe^0@SiO_2$-DI, while only 1.1% for bare Fe^0. The two $Fe@SiO_2$ samples show a better adsorption performance than bare Fe, which may have

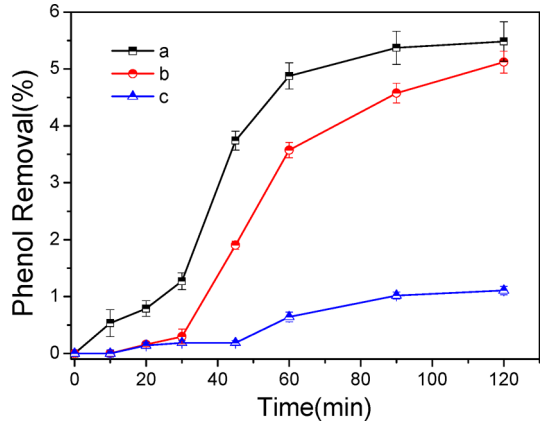

Figure 7. Phenol removal ratio in the absence of H_2O_2: (a) $Fe^0@SiO_2$ YSNs, (b) $Fe^0@SiO_2$-DI, and (c) bare Fe^0.

contributed to the existence of mesoporous silica spheres. Therefore, the HMSS possesses certain adsorption behavior to phenol molecule, confirming the accessibility of the mesoporous shell. In addition, because of the relative lower BET surface area, $Fe^0@SiO_2$-DI exhibits a slight decrease in adsorption of phenol as compared to $Fe^0@SiO_2$ YSNs. Even so, the highest adsorption efficiency of $Fe^0@SiO_2$ YSNs was about 5.5%, indicating that the removal of phenol in the oxidation system mainly contributed to the catalysis reaction. It is further confirmed that the superior catalytic performance can be assigned to the structure-enhanced effect of YSNs nanoreactors, including facilitating mass-transfer and confinement effect.

4. CONCLUSIONS

In summary, yolk−shell structured $Fe^0@SiO_2$ nanoparticles were fabricated via a sequential "two-solvents" impregnation−reduction approach. The as-synthesized $Fe^0@SiO_2$ YSNs show distinctive structures with active cores, perpendicular mesoporous channels, protective shells, and hollow cavities. Attributed to the structure-enhanced effect of YSNs as nanoreactors, $Fe^0@SiO_2$ YSNs have shown excellent performance in Fenton-like reaction toward phenol total degradation with outstanding activity and selectivity. It can be envisioned that the sequential "two-solvents" impregnation−reduction approach may be versatile and could synthesize a wide range of yolk−shell structures with different cores, and we believe that the multiple functionalized YSNs can yield a variety of applications, such as nanoreactors, drug delivery, biosensors, surface-enhanced Raman scattering, and lithium-ion batteries.

■ ASSOCIATED CONTENT

Supporting Information

TEM image of Fe^0, TEM image and wide-angle pattern of Au@silica YSNs, HPLC patterns of reaction process, intermediate products, and standard materials. This material is available free of charge via the Internet at http://pubs.acs.org.

■ AUTHOR INFORMATION

Corresponding Authors

*E-mail: lijsh@mail.njust.edu.cn.

*E-mail: wanglj@mail.njust.edu.cn.

Notes

The authors declare no competing financial interest.

■ ACKNOWLEDGMENTS

This work was financially supported by the National Natural Science Foundation of China (Grant no. 51078184).

■ REFERENCES

(1) Liu, J.; Qiao, S. Z.; Chen, J. S.; Lou, X. W.; Xing, X. R.; Lu, G. Q. Yolk/Shell Nanoparticles: New Platforms for Nanoreactors, Drug Delivery and Lithium-Ion Batteries. *Chem. Commun.* **2011**, *47*, 12578−12591.

(2) Lou, X. W.; Archer, L. A.; Yang, Z. C. Hollow Micro-/Nanostructures: Synthesis and Applications. *Adv. Mater.* **2008**, *21*, 3987−4019.

(3) Perez-Lorenzo, M.; Vaz, B.; Salgueirino, V.; Correa-Duarte, M. A. Hollow-Shelled Nanoreactors Endowed with High Catalytic Activity. *Chem.—Eur. J.* **2013**, *37*, 12196−12211.

(4) Yeo, K. M.; Shin, J.; Lee, I. S. Reductive Dissolution of Fe_3O_4 Facilitated by The Au Domain of an Fe_3O_4/Au Hybrid Nanocrystal: Formation of a Nanorattle Structure Composed of a Hollow Porous Silica Nanoshell and Entrapped Au Nanocrystal. *Chem. Commun.* **2010**, *1*, 64−66.

(5) Sanles-Sobrido, M.; Perez-Lorenzo, M.; Rodriguez-Gonzalez, B.; Salgueirino, V.; Correa-Duarte, M. A. Highly Active Nanoreactors: Nanomaterial Encapsulation Based on Confined Catalysis. *Angew. Chem., Int. Ed.* **2012**, *16*, 3877−3882.

(6) Cui, Z. M.; Chen, Z.; Cao, C. Y.; Jiang, L.; Song, W. G. A Yolk-Shell Structured Fe_2O_3@Mesoporous SiO_2 Nanoreactor for Enhanced Activity as A Fenton Catalyst in Total Oxidation of Dyes. *Chem. Commun.* **2013**, *23*, 2332−2334.

(7) Guo, L. M.; Li, J. T.; Zhang, L. X.; Li, J. B.; Li, Y. S.; Yu, C. C.; Shi, J. L.; Ruan, M. L.; Feng, J. W. A Facile Route to Synthesize Magnetic Particles within Hollow Mesoporous Spheres and Their Performance as Separable $Hg^{(2+)}$ Adsorbents. *J. Mater. Chem.* **2008**, *23*, 2733−2738.

(8) Kim, M.; Park, J. C.; Kim, A.; Park, K. H.; Song, H. Porosity Control of Pd@SiO_2 Yolk-Shell Nanocatalysts by the Formation of Nickel Phyllosilicate and Its Influence on Suzuki Coupling Reactions. *Langmuir* **2012**, *15*, 6441−6447.

(9) Fan, C. M.; Zhang, L. F.; Wang, S. S.; Wang, D. H.; Lu, L. Q.; Xu, A. W. Novel CeO_2 Yolk-Shell Structures Loaded with Tiny Au Nanoparticles for Superior Catalytic Reduction of P-Nitrophenol. *Nanoscale* **2012**, *21*, 6835−6840.

(10) Li, G. L.; Tai, C. A.; Neoh, K. G.; Kang, E. T.; Yang, X. L. Hybrid Nanorattles of Metal Core and Stimuli-Responsive Polymer Shell for Confined Catalytic Reactions. *Polym. Chem.* **2011**, *6*, 1368−1374.

(11) Liu, J.; Yang, H. Q.; Kleitz, F.; Chen, Z. G.; Yang, T. Y.; Strounina, E.; Lu, G. Q.; Qiao, S. Z. Yolk-Shell Hybrid Materials with a Periodic Mesoporous Organosilica Shell: Ideal Nanoreactors for Selective Alcohol Oxidation. *Adv. Funct. Mater.* **2012**, *3*, 591−599.

(12) Park, J. C.; Song, H. Metal@Silica Yolk-Shell Nanostructures as Versatile Bifunctional Nanocatalysts. *Nano Res.* **2011**, *1*, 33−49.

(13) Liu, J.; Xia, H.; Xue, D. F.; Lu, L. Double-Shelled Nanocapsules of V_2O_5-Based Composites as High-Performance Anode and Cathode Materials for Li Ion Batteries. *J. Am. Chem. Soc.* **2009**, *34*, 12086−12087.

(14) Lou, X. W.; Li, C. M.; Archer, L. A. Designed Synthesis of Coaxial SnO_2@Carbon Hollow Nanospheres for Highly Reversible Lithium Storage. *Adv. Mater.* **2009**, *24*, 2536.

(15) Lee, K. T.; Jung, Y. S.; Oh, S. M. Synthesis of Tin-Encapsulated Spherical Hollow Carbon for Anode Material in Lithium Secondary Batteries. *J. Am. Chem. Soc.* **2003**, *19*, 5652−5653.

(16) Zhu, Y. F.; Ikoma, T.; Hanagata, N.; Kaskel, S. Rattle-Type Fe_3O_4@SiO_2 Hollow Mesoporous Spheres as Carriers for Drug Delivery. *Small* **2010**, *3*, 471−478.

(17) Chen, Y.; Chen, H. R.; Zeng, D. P.; Tian, Y. B.; Chen, F.; Feng, J. W.; Shi, J. L. Core/Shell Structured Hollow Mesoporous Nanocapsules: A Potential Platform for Simultaneous Cell Imaging and Anticancer Drug Delivery. *ACS Nano* **2010**, *10*, 6001−6013.

(18) Roca, M.; Haes, A. J. Silica-Void-Gold Nanoparticles: Temporally Stable Surf ace-Enhanced Raman Scattering Substrates. *J. Am. Chem. Soc.* **2008**, *43*, 14273−14279.

(19) Chen, G.; Wang, Y.; Yang, M. X.; Xu, J.; Goh, S. J.; Pan, M.; Chen, H. Y. Measuring Ensemble-Averaged Surface-Enhanced Raman Scattering in the Hotspots of Colloidal Nanoparticle Dimers and Trimers. *J. Am. Chem. Soc.* **2010**, *11*, 3644.

(20) Zhou, L. Z.; Kuai, L.; Li, W. Z.; Geng, B. Y. Ion-Exchange Route to Au-CuxOS Yolk-Shell Nanostructures with Porous Shells and Their Ultrasensitive H_2O_2 Detection. *ACS Appl. Mater. Interfaces* **2012**, *12*, 6463−6467.

(21) Zhu, Y. F.; Kockrick, E.; Ikoma, T.; Hanagata, N.; Kaskel, S. An Efficient Route to Rattle-Type Fe_3O_4@SiO_2 Hollow Mesoporous Spheres Using Colloidal Carbon Spheres Templates. *Chem. Mater.* **2009**, *12*, 2547−2553.

(22) Liu, G. Y.; Yang, X. L.; Wang, Y. M. Synthesis of Ellipsoidal Hematite/Silica/Polymer Hybrid Materials and the Corresponding Hollow Polymer Ellipsoids. *Langmuir* **2008**, *10*, 5485−5491.

(23) Yang, H. G.; Zeng, H. C. Creation of Intestine-Like Interior Space for Metal-Oxide Nanostructures with a Quasi-Reverse Emulsion. *Angew. Chem., Int. Ed.* **2004**, *39*, 5206−5209.
(24) Li, J.; Zeng, H. C. Hollowing Sn-Doped $TiO_{(2)}$ Nanospheres via Ostwald Ripening. *J. Am. Chem. Soc.* **2007**, *51*, 15839−15847.
(25) Sun, Y. G.; Wiley, B.; Li, Z. Y.; Xia, Y. N. Synthesis and Optical Properties of Nanorattles and Multiple-Walled Nanoshells/Nanotubes Made of Metal Alloys. *J. Am. Chem. Soc.* **2004**, *30*, 9399−9406.
(26) Gao, J. H.; Liang, G. L.; Zhang, B.; Kuang, Y.; Zhang, X. X.; Xu, B. FePt@CoS_2 Yolk-Shell Nanocrystals as a Potent Agent to Kill HeLa Cells. *J. Am. Chem. Soc.* **2007**, *5*, 1428−1433.
(27) Wang, D. P.; Zeng, H. C. Multifunctional Roles of TiO_2 Nanoparticles for Architecture of Complex Core-Shells and Hollow Spheres of SiO_2-TiO_2-Polyaniline System. *Chem. Mater.* **2009**, *20*, 4811−4823.
(28) Goebl, J.; Yin, Y. D. Ship in a Bottle: In situ Confined Growth of Complex Yolk-shell Catalysts. *ChemCatChem* **2013**, *6*, 1287−1288.
(29) Liu, J.; Liu, F.; Gao, K.; Wu, J. S.; Xue, D. F. Recent Developments in the Chemical Synthesis of Unorganic Porous Capsules. *J. Mater. Chem.* **2009**, *34*, 6073−6084.
(30) Chen, D.; Li, L. L.; Tang, F. Q.; Qi, S. O. Facile and Scalable Synthesis of Tailored Silica "Nanorattle" Structures. *Adv. Mater.* **2009**, *37*, 3804−3807.
(31) Chen, Y.; Chen, H. R.; Ma, M.; Chen, F.; Guo, L. M.; Zhang, L. X.; Shi, J. L. Double Mesoporous Silica Shelled Spherical/Ellipsoidal Nanostructures: Synthesis and Hydrophilic/Hydrophobic Anticancer Drug Delivery. *J. Mater. Chem.* **2011**, *14*, 5290−5298.
(32) Hah, H. J.; Um, J. I.; Han, S. H.; Koo, S. M. New Synthetic Route for Preparing Rattle-Type Silica Particles with Metal Cores. *Chem. Commun.* **2004**, *8*, 1012−1013.
(33) Tan, L. F.; Chen, D.; Liu, H. Y.; Tang, F. Q. A Silica Nanorattle with a Mesoporous Shell: An Ideal Nanoreactor for the Preparation of Tunable Gold Cores. *Adv. Mater.* **2010**, *43*, 4885.
(34) Ding, S. J.; Chen, J. S.; Qi, G. G.; Duan, X. N.; Wang, Z. Y.; Giannelis, E. P.; Archer, L. A.; Lou, X. W. Formation of SnO_2 Hollow Nanospheres inside Mesoporous Silica Nanoreactors. *J. Am. Chem. Soc.* **2011**, *1*, 21−23.
(35) Imperor-Clerc, M.; Bazin, D.; Appay, M. D.; Beaunier, P.; Davidson, A. Crystallization of Beta-MnO_2 Nanowires in the Pores of SBA-15 Silicas: In Situ Investigation Using Synchrotron Radiation. *Chem. Mater.* **2004**, *9*, 1813−1821.
(36) van der Meer, J.; Bardez-Giboire, I.; Mercier, C.; Revel, B.; Davidson, A.; Denoyel, R. Mechanism of Metal Oxide Nanoparticle Loading in SBA-15 by the Double Solvent Technique. *J. Phys. Chem. C* **2010**, *8*, 3507−3515.
(37) Jiao, K.; Zhang, B.; Yue, B.; Ren, Y.; Liu, S. X.; Yan, S. R.; Dickinson, C.; Zhou, W. Z.; He, H. Y. Growth of Porous Single-Crystal Cr_2O_3 in a 3-D Mesopore System. *Chem. Commun.* **2005**, *45*, 5618−5620.
(38) Kleitz, F.; Choi, S. H.; Ryoo, R. Cubic Ia3d Large Mesoporous Silica: Synthesis and Replication to Platinum Nanowires, Carbon Nanorods and Carbon Nanotubes. *Chem. Commun.* **2003**, *17*, 2136−2137.
(39) van der Meer, J.; Bardez, I.; Bart, F.; Albouy, P. A.; Wallez, G.; Davidson, A. Dispersion of Co_3O_4 Nanoparticles within SBA-15 Using Alkane Solvents. *Microporous Mesoporous Mater.* **2009**, *1*−*3*, 183−188.
(40) Lu, Q. S.; Wang, Z. Y.; Li, J. G.; Wang, P. Y.; Ye, X. L. Structure and Photoluminescent Properties of ZnO Encapsulated in Mesoporous Silica SBA-15 Fabricated by Two-Solvent Strategy. *Nanoscale Res. Lett.* **2009**, *7*, 646−654.
(41) Roggenbuck, J.; Waitz, T.; Tiemann, M. Synthesis of Mesoporous Metal Oxides by Structure Replication: Strategies of Impregnating Porous Matrices with Metal Salts. *Microporous Mesoporous Mater.* **2008**, *1*−*3*, 575−582.
(42) Lopes, I.; Davidson, A.; Thomas, C. Calibrated Co_3O_4 Nanoparticles Patterned in SBA-15 Silicas: Accessibility and Activity for CO Oxidation. *Catal. Commun.* **2007**, *12*, 2105−2109.
(43) Laugel, G.; Arichi, J.; Guerba, H.; Moliere, M.; Kiennemann, A.; Garin, F.; Louis, B. Co_3O_4 and Mn_3O_4 Nanoparticles Dispersed on SBA-15: Efficient Catalysts for Methane Combustion. *Catal. Lett.* **2008**, *1*−*2*, 14−21.
(44) Teng, Z. G.; Su, X. D.; Zheng, Y. Y.; Sun, J.; Chen, G. T.; Tian, C. C.; Wang, J. D.; Li, H.; Zhao, Y. N.; Lu, G. M. Mesoporous Silica Hollow Spheres with Ordered Radial Mesochannels by a Spontaneous Self-Transformation Approach. *Chem. Mater.* **2013**, *1*, 98−105.
(45) Bagshaw, S. A.; Prouzet, E.; Pinnavaia, T. J. Templating of Mesoporous Molecular Sieves by Nonionic Polyethylene Oxide Surfactants. *Science* **1995**, *269*, 1242−1244.
(46) Kim, S. S.; Pauly, T. R.; Pinnavaia, T. J. Non-ionic Surfactant Assembly of Wormhole Silica Molecular Sieves from Water Soluble Silicates. *Chem. Commun.* **2000**, 835−836.
(47) Grosvenor, A. P.; Kobe, B. A.; Biesinger, M. C.; McIntyre, N. S. Investigation of Multiplet Splitting of Fe 2p XPS Spectra and Bonding in Iron Compounds. *Surf. Interface Anal.* **2004**, *12*, 1564−1574.
(48) Nurmi, J. T.; Tratnyek, P. G.; Sarathy, V.; Baer, D. R.; Amonette, J. E.; Pecher, K.; Wang, C. M.; Linehan, J. C.; Matson, D. W.; Penn, R. L.; Driessen, M. D. Characterization and Properties of Metallic Iron Nanoparticles: Spectroscopy, Electrochemistry, and Kinetics. *Environ. Sci. Technol.* **2005**, *5*, 1221−1230.
(49) Pera-Titus, M.; Garcia-Molina, V.; Banos, M. A.; Gimenez, J.; Esplugas, S. Degradation of Chlorophenols by Means of Advanced Oxidation Processes: A General Review. *Appl. Catal., B* **2004**, *4*, 219−256.
(50) Navalon, S.; Alvaro, M.; Garcia, H. Heterogeneous Fenton Catalysts Based on Clays, silicas and zeolites. *Appl. Catal., B* **2010**, *1*−*2*, 1−26.
(51) Bremner, D. H.; Burgess, A. E.; Houllemare, D.; Namkung, K. C. Phenol Degradation Using Hydroxyl Radicals Generated from Zero-Valent Iron and Hydrogen Peroxide. *Appl. Catal., B* **2006**, *1*−*2*, 15−19.
(52) Dhakshinamoorthy, A.; Navalon, S.; Alvaro, M.; Garcia, H. Metal Nanoparticles as Heterogeneous Fenton Catalysts. *ChemSusChem* **2012**, *1*, 46−64.
(53) Liu, J.; Qiao, S. Z.; Hartono, S. B.; Lu, G. Q. Monodisperse Yolk-Shell Nanoparticles with a Hierarchical Porous Structure for Delivery Vehicles and Nanoreactors. *Angew. Chem., Int. Ed.* **2010**, *29*, 4981−4985.